Diffusive and Convective Protein Transport through Asymmetric Membranes

W. Senyo Opong and Andrew L. Zydney
Dept. of Chemical Engineering, University of Delaware, Newark, DE 19716

Experimental data are obtained for bovine serum albumin transport through asymmetric polyethersulfone ultrafiltration membranes of differing molecular weight cutoff in a stirred ultrafiltration device. The actual membrane sieving coefficient is determined from filtrate concentration measurements using a stagnant film model to account for bulk mass transport effects. These sieving coefficients are then used to evaluate the relative contributions of diffusive and convective transport to the overall protein flux. The results are in good agreement with available hydrodynamic models for the hindrance factors for convective and diffusive transport of spherical solutes through well-defined pores, with the effective solute to pore size ratio evaluated from a partitioning model that explicitly accounts for the ellipsoidal shape of the protein and the membrane pore size distribution. The implications of these results to the analysis of experimental data for membrane sieving and to the design of effective protein fractionation devices are also discussed.

Introduction

Membrane ultrafiltration has become an increasingly important industrial process for the concentration and purification of protein solutions. Most experimental and theoretical studies of ultrafiltration have focused on systems in which the membranes are either totally retentive or fully permeable to the solutes of interest. There has been relatively little work on macromolecular transport through partially retentive membranes, despite its potential importance in separations of multicomponent protein solutions (for example, bioreactor effluents) and in the specific fractionation of solutions containing two or more proteins. The lack of effective separation in previous studies of selective protein filtration, such as the separation of albumin (MW = 69,000) from immunoglobulins (MW = 155,000) (Sieberth et al., 1983; Oda and Inoue, 1983), has often been attributed to the inadequate transport characteristics of available ultrafiltration membranes, even though there is little, if any, fundamental data available on macromolecular transport through the asymmetric membranes used in these clinical and industrial applications.

The objective of this study was to obtain quantitative data on combined convective and diffusive transport of bovine serum albumin (BSA) through the highly constricted pores of asymmetric ultrafiltration membranes with a range of nominal molecular weight cutoffs. Experimental data for BSA sieving as a function of filtrate flux were obtained using a stirred ultrafiltration cell, with the effects of concentration polarization evaluated using a stagnant film model. This made it possible to determine the diffusive and convective contributions to BSA transport from data obtained during a single experimental run. The experimental results were then compared with predictions of hydrodynamic theory to examine the applicability of available hydrodynamic models, which are strictly limited to the transport of spherical solutes in well-defined pores, to describe protein transport through the highly constricted pores in asymmetric ultrafiltration membranes.

Theoretical Background

Three distinct theoretical approaches have been used to describe transport in porous membranes: the Kedem-Katchalsky analysis (Kedem and Katchalsky, 1958; Spiegler and Kedem, 1966); the Stefan-Maxwell multicomponent diffusion equations (Lightfoot, 1974; Robertson, 1989); and hydrodynamic models (Anderson and Quinn, 1974; Deen, 1987). The first two approaches are developed directly from the principles of irreversible thermodynamics; they both lead to a set of phenomenological equations relating the solute and solvent fluxes to gradients in the pressure and concentration driving forces.

Correspondence concerning this article should be addressed to A. Zydney.

In contrast, hydrodynamic models evaluate the solute flux by directly solving the governing hydrodynamic equations for the motion of a single solute in a well-defined pore, with the resulting transport parameters expressed directly in terms of the solute and pore characteristics. In all three approaches, the solute flux through the membrane (N_s) is given by the sum of the convective and diffusive contributions:

$$N_s = K_c V C_s - K_d D_\infty \frac{dC_s}{dz} \tag{1}$$

where C_s is the radially averaged solute concentration in the pore, V is the radially averaged solution velocity, and D_∞ is the free solution Brownian motion diffusivity. K_c and K_d are the hindrance factors for convective and diffusive transport, respectively. They both reflect the additional drag on the solute molecule due to the presence of the pore walls.

Equation 1 can be integrated across the membrane, with the solute concentrations in the membrane at the upper ($z=0$) and lower ($z=\delta_m$) surfaces expressed in terms of the external concentrations (C_w and C_f) using the equilibrium partition coefficient:

$$\phi = \frac{C_s(z=0)}{C_w} = \frac{C_s(z=\delta_m)}{C_f} \tag{2}$$

The results are conveniently expressed in terms of the actual sieving coefficient (S_a), defined as the ratio of the solute concentration in the filtrate (C_f) to that at the upper surface of the membrane (C_w) (Anderson and Quinn, 1974; Spiegler and Kedem, 1966):

$$S_a = \frac{C_f}{C_w} = \frac{S_\infty \exp(Pe_m)}{S_\infty + \exp(Pe_m) - 1} \tag{3}$$

where

$$S_\infty = \phi K_c \tag{4}$$

is the asymptotic value of the sieving coefficient attained at infinite Peclet numbers (Pe_m):

$$Pe_m = \left(\frac{K_c}{K_d}\right)\left(\frac{V\delta_m}{D_\infty}\right) = \left(\frac{S_\infty}{\phi K_d}\right)\left(\frac{V\delta_m}{D_\infty}\right) \tag{5}$$

with δ_m the membrane thickness. The second equality in Eq. 5 is developed by substitution of Eq. 4; the quantity ϕK_d is simply equal to the ratio of the effective diffusion coefficient through the membrane (D_{eff}) to that in free solution. At small Peclet numbers, solute transport is governed primarily by diffusion, thus the solute concentrations on the two sides of the membrane become nearly equal and the sieving coefficient approaches unity. Equation 3 was originally developed by Spiegler and Kedem (1966) in terms of the membrane rejection coefficient:

$$R = 1 - S_a \tag{6}$$

with the asymptotic value of the rejection coefficient at large Pe_m equal to the Staverman reflection coefficient, σ_0. Equation 3 has also been developed using the Stefan-Maxwell equations (Robertson and Zydney, 1988) with S_∞ and ϕK_d given in terms of the Stefan-Maxwell diffusivities.

Hydrodynamic analyses

Deen (1987) has recently reviewed the previous work on hydrodynamic analyses of hindered transport, thus the following discussion will consider only those points most pertinent to our analysis. Although general approaches for the analysis of hindered transport of rigid solutes in pores of arbitrary shape have been developed (Anderson and Quinn, 1974; Brenner and Gaydos, 1977), the necessary hydrodynamic coefficients are unavailable even for relatively simple axisymmetric solutes or pores. Analytical expressions have been developed for spherical solutes in cylindrical pores using the centerline approximation (Lane, 1950; Renkin, 1954; Anderson and Quinn, 1974; Bungay and Brenner, 1973). Bungay and Brenner (1973) developed expressions for K_c and K_d which are valid for all values of the ratio of the solute (R_s) to pore (R_p) radii (λ) using matched asymptotic expansions for both small and close fitting spheres yielding:

$$K_d = \frac{6\pi}{K_t} \tag{7}$$

$$K_c = \frac{(2-\phi)K_s}{2K_t} \tag{8}$$

where the equilibrium partition coefficient (ϕ) for a spherical solute in a cylindrical pore is simply (Renkin, 1954; Giddings et al., 1968):

$$\phi = (1-\lambda)^2 \tag{9}$$

The functions K_s and K_t are both expressed as expansions in λ:

$$\begin{pmatrix} K_t \\ K_s \end{pmatrix} = \frac{9}{4}\pi^2\sqrt{2}(1-\lambda)^{-5/2}\left[1 + \sum_{n=1}^{2}\begin{pmatrix} a_n \\ b_n \end{pmatrix}(1-\lambda)^n\right] + \sum_{n=0}^{4}\begin{pmatrix} a_{n+3} \\ b_{n+3} \end{pmatrix}\lambda^n \tag{10}$$

with the coefficients a_n and b_n given in Table 1. Equations 7 to 10 are in good agreement with more rigorous analyses of hindered diffusion valid for $\lambda < 0.1$ (Brenner and Gaydos, 1977)

Table 1. Expansion Coefficients for Hydrodynamic Functions K_s and K_t in Eq. 10

Subscript n	a_n	b_n
1	−73/60	7/60
2	77,293/50,400	−2,227/50,400
3	−22.5083	4.0180
4	−5.6117	−3.9788
5	−0.3363	−1.9215
6	−1.216	4.392
7	1.647	5.006

and $\lambda > 0.9$ (Mavrovouniotis and Brenner, 1988) developed by explicitly averaging the local solute concentration in the pore over the radial direction. More recent analyses have extended these results to include the effects of solute concentration (Adamski and Anderson, 1983; Mitchell and Deen, 1986) and electrostatic interactions (Smith and Deen, 1983; Mitchell and Deen, 1984).

Analytical results for K_d and K_c for slit-shaped pores are more limited, but expansions have been obtained for spherical solutes using the centerline approximation (Happel and Brenner, 1983):

$$K_d = 1 - 1.004\lambda + 0.418\lambda^3 + 0.21\lambda^4 - 0.169\lambda^5 + O(\lambda^6) \quad (11)$$

$$K_c = \frac{3-\phi^2}{2}\left(1 - \frac{\lambda^2}{3} + O(\lambda^3)\right) \quad (12)$$

where $\lambda = R_s/h$ with h the slit half-width. In this case, the partition coefficient is given as:

$$\phi = 1 - \lambda \quad (13)$$

Although general analytical expressions for the hindrance factors and partition coefficient for nonspherical solutes in pores of arbitrary geometry are unavailable, Giddings et al. (1968) showed that the partitioning behavior of a wide range of solutes in different pore geometries was governed primarily by the quantity:

$$\lambda^* = R^*/2s \quad (14)$$

where R^* is the mean projected solute radius ($R^* = R_s$ for a sphere) and s is the specific area of the pore, equal to the pore volume (V_p) divided by the pore surface area (S_p). Giddings et al.'s formulation has been shown to be in good agreement with Monte Carlo calculations of the partitioning of rigid, nonspherical particles in pores of several different geometries (Limbach et al., 1989). For rigid solutes in an isotropic porous network formed by a random arrangement of parallel planes, Giddings et al. (1968) showed that the partition coefficient was given as:

$$\phi = \exp(-2\lambda^*) \quad (15)$$

independent of the solute geometry.

Comparison with experimental data

Most experimental studies of hindered transport have employed track-etched polycarbonate membranes with uniform well-defined cylindrical pores or track-etched mica membranes with rhomboidal pores. Experimental data for the hindered diffusion coefficient for ficoll (Deen et al., 1981; Bohrer et al., 1984), a variety of small macromolecules (Beck and Schultz, 1972) and asphaltenes (Baltus and Anderson, 1983) were all in relatively good agreement with available hydrodynamic models, although the data were limited primarily to large pores ($\lambda < 0.5$). Results for protein diffusion are more limited. Wong and Quinn (1976) obtained data for BSA diffusion through mica membranes, which indicated that the effective pore size was reduced by a monolayer of adsorbed BSA. However, even when this adsorbed layer was taken into account, the data were about a factor of two smaller than predicted. Subsequent studies of BSA partitioning suggested that this discrepancy was due to electrostatic effects (Rodilosso, 1984), although the details of the adsorbed BSA layer, the rhomboidal pore geometry, and the ellipsoidal shape of the albumin molecule (39 Å × 139 Å) may also have contributed to these results.

Experimental data for convective transport (that is, for S_∞) are more scattered and show much greater discrepancies with hydrodynamic models. For example, Zeman and Wales (1981) and Long et al. (1981) reported data for S_∞ for dextrans which were in relatively good agreement with theoretical predictions, while Mitchell and Deen (1986) reported data that were much smaller than predicted. Experimental data for BSA sieving (Munch et al., 1979; Mitchell and Deen, 1986) indicate that BSA adsorption reduces the effective pore size, and Mitchell and Deen (1984) have demonstrated that electrostatic interactions may also be important. But even when these effects were taken into account, the results were smaller than the predicted values by as much as a factor of two even for relatively large pores (λ between 0.1 and 0.2). Schultz et al. (1979) evaluated S_∞ for BSA and IgG from measurements of the osmotic reflection coefficient (σ_o), with $S_\infty \approx 1 - \sigma_o$ (Anderson, 1981), but the data were highly scattered making it difficult to draw any definite conclusions regarding the accuracy of the hydrodynamic predictions. The reason for this discrepancy in the results for solute sieving has not been clarified.

In addition to these studies with track-etched membranes, there have also been a few important investigations of solute transport through asymmetric ultrafiltration membranes. Nakao and Kimura (1981) evaluated the actual sieving coefficient for small solutes (molecular weight from 90 to 3,000) through cellulose acetate membranes. The flux dependence for S_a was in good agreement with Eq. 3 allowing the evaluation of both S_∞ and ϕK_d. The S_∞ values for different solutes were well described using hydrodynamic models, with the effective pore radius evaluated by fitting the S_∞ data to the model. In contrast, the results for ϕK_d were in poor agreement with theory, which Nakao and Kimura (1981) attributed to the extensive pore connectivity in the cellulose acetate membranes. The diffusion data were instead fit to available hydrodynamic models with the effective pore length assumed to be a function of solute size. The results were well described by an inverse dependence of pore length on the cube of the solute diameter, although there is no independent justification for this type of dependence.

Tsapuik et al. (1990) recently measured the sieving coefficient of several small solutes (MW 92 to 342) and polyethylene glycols (MW 400 to 40,000) through cellulose acetate, polysulfonamide, and track-etched polyethylene terephthalate membranes. The results were consistent with the flux dependence given by Eq. 3. No comparison with hydrodynamic theory was presented. Instead, Tsapuik et al. (1990) analyzed the data by assuming that $S_\infty = \phi$ and that $D_{eff}/D_\infty = \phi^2$. The effective membrane thickness (δ_m) was then evaluated from the sieving data for each solute using Eq. 3. δ_m decreased with increasing solute molecular weight for the cellulose acetate membranes, but was independent of molecular weight for the track-etched membrane. It is difficult to draw any definite conclusions from these results, since the assumption that $S_\infty = \phi$ neglects any hindrance effects on convection and the assumption that

$D_{eff}/D_\infty = \phi^2$ is not strictly consistent with any available hydrodynamic analyses.

Robertson and Zydney (1990b) recently obtained data for BSA diffusion through the same polyethersulfone membranes used in this study. The diffusion coefficient in the membrane skin was evaluated by subtracting off the contributions from the membrane support structure. Robertson and Zydney (1988) also obtained data for BSA sieving in an unstirred batch filtration device for a 50,000-molecular-weight cutoff membrane, which indicated that the flux dependence for S_a was well described by Eq. 3. These results are discussed in more detail in conjunction with the data obtained in the current investigation.

In summary, experimental data for hindered transport through partially permeable asymmetric ultrafiltration membranes are highly limited, with the work by Nakao and Kimura (1981) and more recently by Tsapuik et al. (1990) confined to small solutes and flexible polymers. Essentially no results are available for globular proteins like BSA. In addition, these previous studies provide little guidance as to whether available hydrodynamic models can be used to describe protein transport through the highly constricted and irregular pores in asymmetric membranes or how to best define the effective solute and pore size under these conditions.

The objectives of this work were (a) to obtain quantitative data for BSA transport through asymmetric ultrafiltration membranes as a function of flux; (b) to use the data to evaluate the hydrodynamic parameters describing convective (S_∞) and diffusive (ϕK_d) solute transport; and (c) to determine if available hydrodynamic models for the transport of spherical solutes through well-defined pores can provide an accurate description of protein transport through asymmetric ultrafiltration membranes using appropriate definitions for the effective solute and pore size.

Materials and Methods

All ultrafiltration experiments were performed with solutions of bovine serum albumin with concentrations from 1 to 25 g/L. The solutions were prepared by dissolving BSA powder (Cohn fraction V, Sigma Chemicals) in 0.15 M NaCl that had been prefiltered through a 1,000,000 (1-M)-molecular-weight cutoff polyethersulfone membrane (Filtron Corporation, Northborough, MA). The solution pH was adjusted to 6.8–7.0 using small amounts of 0.1-M NaOH or HCl as required. The protein solutions were then prefiltered through a 100,000 (100-K) molecular weight cutoff membrane (a 1-M membrane was used for the 25-g/L solution) prior to use. Microscopic observation of the filtered BSA solutions confirmed that they were free of aggregates and micro-organisms. The BSA solutions were stored at 4°C and used within 2 days of preparation.

Protein concentrations were determined spectrophotometrically by reaction of BSA with bromcresol green (Sigma Chemicals). The absorbance of the resulting blue-green complex was measured at 628 nm using a Perkin-Elmer Lambda 4B Spectrophotometer (Perkin Elmer, Norwalk, CT) and compared to that of BSA standards of known concentration. Protein concentrations could be measured accurately to within ±0.1 g/L.

The majority of the protein filtration experiments were performed using OMEGA polyethersulfone ultrafiltration membranes, provided by Filtron Corporation (Northborough, MA), with molecular weight cutoffs ranging from 50,000 to 1,000,000. These membranes are anisotropic consisting of: (1) an ultrathin functional polyethersulfone skin (approximately 0.5 μm thick), which determines the sieving properties of the membrane; (2) a porous polyethersulfone substructure (approximately 50 μm thick); and (3) a porous support matrix (approximately 230 μm thick) made of Tyvek (DuPont Co., Wilmington, DE). In addition, limited experimental data were obtained with 0.01-μm track-etched polycarbonate membranes (Poretics, Livermore, CA) with well-defined cylindrical pores (approximately 6 μm thick). All membranes were flushed with filtered deionized distilled water prior to use (this removed the glycerine used as a wetting agent in the polyethersulfone membranes) using at least 100 L of water per m^2 of membrane area.

Previous data for BSA adsorption to the polyethersulfone membranes indicated that equilibrium adsorption was not attained until after 10 to 12 hours due to diffusional limitations within the porous membrane (Robertson and Zydney, 1990a). All membranes were thus soaked in a BSA solution of the same concentration as that to be used in the sieving experiments for approximately 24 h at 4°C prior to use. The membrane was then gently rinsed in 0.15-M saline to remove any labile protein, and the hydraulic permeability was evaluated as described below.

Protein filtration

All filtration experiments were conducted using a 25-mm-diameter Amicon UF cell (Model 8010, Amicon Corporation, Danvers, MA) connected to a 1-L reservoir containing either the saline or protein solution. The transmembrane pressure was set by adjusting the height of the solution reservoir (for pressures less than 14 kPa, 2 psi) or by air pressurization of the reservoir. The pressure on the filtrate side was approximately atmospheric under all conditions. All experiments were conducted at room temperature (22 ± 3°C).

The membrane was mounted in the stirred cell and the entire apparatus was carefully filled with saline to eliminate any entrapped air bubbles in the cell and associated tubing. The hydraulic permeability of the membrane was evaluated by measuring the saline flow rate via timed collection as a function of applied pressure. The filtrate port was then clamped, the saline solution replaced with a protein solution, and the desired applied pressure established by adjusting the reservoir height or the air pressure regulator. The stirrer was then set at the desired rotational speed (previously calibrated using a strobe light), after which the feed and filtrate ports were unclamped. Data collection was begun after the system attained stable operation, that is, after filtration for a minimum of 2 minutes and after collection of a minimum of 500 μL of filtrate, with the latter required to wash out the dead volume downstream of the membrane in the stirred cell (approximately 200 μL). Filtrate flow rates were evaluated using timed collection with the filtrate mass determined using a Sartorius digital balance with accuracy of ±1 mg (Model 1518 Sartorius, Westbury, NY). The BSA concentration in the filtrate was determined spectrophotometrically as described previously. Results are reported as the mean of three consecutive measurements obtained for each set of experimental conditions. In all cases, the three repeat measurements for both flux and concentration were within 8%.

The filtrate port was then clamped and a small sample (approximately 100 μL) was taken directly from the stirred cell to evaluate the bulk protein concentration. The stirred cell was then emptied and refilled with saline. The saline flux was re-evaluated, with the experiments continued only if the flux differed by less than 5% from the value determined at the start of the experimental run. The protein solution was then returned to the stirred cell and the entire procedure repeated at a new applied pressure. To minimize protein deposition, data were obtained by monotonically increasing the flux (by increasing the applied pressure), with several data points obtained at the end of the run at a low flux to verify that there were no changes in membrane properties during the experimental run.

Experimental data for the filtrate concentration were used to evaluate the actual membrane sieving coefficient (S_a) by accounting for the effects of concentration polarization, the formation of a concentration boundary layer above the membrane. The complex hydrodynamics in the stirred cell do not permit the development of an analytical solution for the protein concentration profiles above the membrane, thus a stagnant film model (Blatt et al., 1970) was used to relate the actual sieving coefficient ($S_a = C_f/C_w$) to the observed sieving coefficient ($S_o = C_f/C_b$):

$$S_a = \frac{S_o}{(1 - S_o)\exp(J_v/k) + S_o} \tag{16}$$

where J_v is the superficial velocity ($J_v = \epsilon V$ with ϵ the membrane porosity) and k is the mass transfer coefficient averaged over the membrane surface. Experimental measurements of the rate of benzoic acid dissolution (Smith et al., 1968) and the rate of solute diffusion across mica membranes (Malone and Anderson, 1977) indicate that for laminar flow ($Re < 32{,}000$, which corresponds to $\omega < 2{,}300$ rpm in our system) the mass transfer coefficient is given as:

$$\frac{kr}{D_\infty} = \Psi Re^{0.567} Sc^{0.33} \tag{17}$$

where $Re = \omega r^2/\nu$ is the Reynolds number, $Sc = \nu/D_\infty$ the Schmidt number, r the radius of the stirred cell, ω the stirring speed, and ν the kinematic viscosity. Equations 16 and 17 have also been used by Mitchell and Deen (1986) in their analysis of BSA rejection by track-etched polycarbonate membranes, with the Re exponent evaluated as 0.537 using a polarographic technique. The coefficient Ψ is a function of device geometry (Smith et al., 1968) and possibly membrane porosity (Malone and Anderson, 1977). We evaluated the parameter Ψ by comparison of experimental data for the filtrate flux for BSA solutions through highly retentive membranes with model calculations as described in the Appendix. The results gave $\Psi = 0.23$, about 17% less than the value given by the correlation developed by Smith et al. (1968).

Results and Analysis

Experimental data for the observed (upper panel) and actual (lower panel) sieving coefficients for filtration of a 5-g/L BSA solution through an OMEGA 100-K membrane at a stirring speed of 600 rpm are shown as a function of filtrate flux (J_v) in Figure 1. The actual sieving coefficients were evaluated directly from the data for S_o at each filtrate flux using the stagnant film model (Eq. 16), with the mass transfer coefficient at 600 rpm calculated from Eq. 17 as $k = 5.2 \times 10^{-6}$ m/s. All the data in Figure 1 were obtained with a single OMEGA 100-K membrane used on two separate days, with the membrane stored in 0.15-M NaCl at 4°C in-between the two runs (approximately 48 h). The data obtained from these two runs were in excellent agreement, indicating that protein deposition or membrane fouling was negligible under these experimental conditions. This was also consistent with the saline flux data obtained between the different filtrate concentration measurements, all of which were within ±3%. Scanning electron micrographs of the membranes obtained before and after filtration also showed that these membranes remained free of any protein deposit or microorganisms. In contrast, earlier experiments performed using unfiltered BSA solutions showed a substantial decline in saline flux over time due to protein

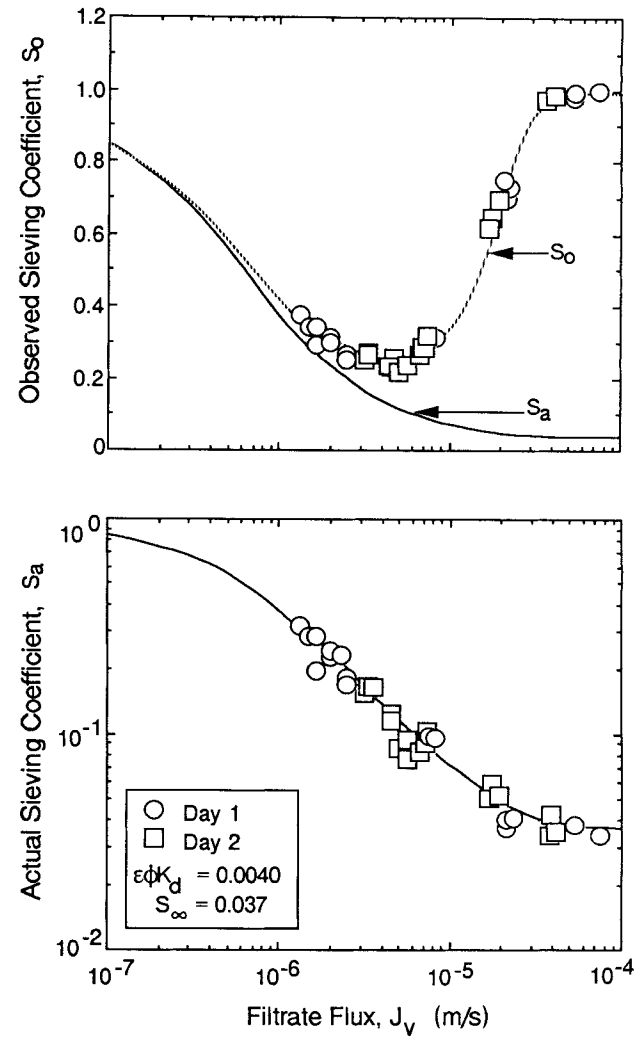

Figure 1. Observed (top panel) and actual (bottom panel) sieving coefficients vs. filtrate flux for a single 100-K membrane used on two separate days.

Solid curves represent model fit with parameters shown. $C_b = 5$ g/L and $k = 5.2 \times 10^{-6}$ m/s.

Table 2. Transport Parameters for Different OMEGA 100-K Membranes

Membrane	C_b (g/L)	ω (rpm)	L_p ($m \times 10^{12}$)	S_∞	$\epsilon\phi K_d$ ($\times 10^2$)	Correlation Coefficient	Mean Deviation (E)
A	5	600	2.0	0.037 ± 0.004	0.40 ± 0.02	0.67	0.08
	5	1,300	2.0	0.060 ± 0.003	0.39 ± 0.04	0.65	0.13
	10	1,300	2.0	0.021 ± 0.01	0.59 ± 0.15	0.87	0.08
	25	1,300	2.0	0.041 ± 0.02	0.42 ± 0.16	0.94	0.04
B	3.5	600	2.8	0.023 ± 0.01	0.55 ± 0.04	0.90	0.05
C	1.2	600	3.5	0.12 ± 0.01	0.70 ± 0.04	0.88	0.03

deposition on the upper surface of the membrane (Opong and Zydney, 1991).

The solid and dashed curves in Figure 1 represent the calculated values of S_a and S_o, respectively, evaluated from Eqs. 3 and 16 using the best fit values of S_∞ and $\epsilon\phi K_d$. These best fit values were determined by minimizing the sum of the squared residuals between predicted and experimental values for S_o using the method of steepest descent. The membrane porosity (ϵ) multiplies ϕK_d since the results are expressed in terms of the filtrate flux (J_v), instead of the average solution velocity in the pore ($V = J_v/\epsilon$). The actual value of $\epsilon\phi K_d$ was determined using a free solution diffusion coefficient of $D_\infty = 6.7 \times 10^{-11}$ m^2/s at 25°C (Keller et al., 1971) and a membrane skin thickness of $\delta_m = 0.5$ μm as provided by the manufacturer. The possible effects of the membrane substructure and matrix on these results are discussed subsequently.

The fitted curves for S_a and S_o are both in good agreement with the experimental data over the entire range of filtrate flux, indicating that Eq. 3 accurately describes the flux dependence of the actual membrane sieving coefficient and that Eq. 16 accurately describes the concentration polarization phenomenon in the stirred cell with $k = 5.2 \times 10^{-6}$ m/s. The actual sieving coefficient decreases with increasing flux, approaching its asymptotic value $S_\infty = 0.037$ above $J_v \approx 10^{-4}$ m/s due to the reduction in the contribution of solute diffusion relative to convection. The observed sieving coefficient is approximately equal to the actual sieving coefficient at low flux, but then begins to peel away from S_a due to the increase in the extent of concentration polarization with increasing flux. The observed sieving coefficient goes through a minimum at a filtrate flux of about 5×10^{-6} m/s, before increasing to essentially unity above a flux of about 3×10^{-5} m/s due to the high degree of polarization. Note that for this run, the minimum value of the observed sieving coefficient, $S_o \approx 0.2$, is almost an order of magnitude larger than the asymptotic sieving coefficient ($S_\infty = 0.037$). Thus, for the OMEGA 100-K membrane it is impossible to measure directly S_∞ without employing substantially higher stirring speeds (corresponding to substantially larger mass transfer coefficients). This effect is discussed in more detail subsequently.

Table 2 summarizes the results for S_∞ and $\epsilon\phi K_d$ for several OMEGA 100-K membranes, all cut from a single large flat sheet. The best fit values for S_∞ and $\epsilon\phi K_d$ were determined as before with the mass transfer coefficients evaluated from Eq. 17. The standard deviations in the fitted parameters were all quite small. The correlation coefficients between the parameters were generally less than 0.9 (except for the run at 25 g/L) indicating that both S_∞ and $\epsilon\phi K_d$ could be accurately determined from the filtrate concentration data obtained in the stirred cell. The mean square deviations between the experimental and calculated values for the observed sieving coefficient weighted by the experimental values,

$$E = \sqrt{\frac{1}{N}\sum_{i=1}^{N}\left(\frac{S_{o,\text{exp}} - S_{o,\text{calc}}}{S_{o,\text{exp}}}\right)^2} \tag{18}$$

were all less than 15% (and were generally less than 8%), again indicating that Eqs. 3 and 16 accurately describe the flux dependence of the observed sieving coefficient with the mass transfer coefficient given by Eq. 17 with $\Psi = 0.23$.

The data for membrane A at 1,300 rpm were obtained several weeks after the runs at 600 rpm (data shown in Figure 1), with the membrane stored in 0.15-M NaCl at 4°C between these experiments. The variability in the values of S_∞ and $\epsilon\phi K_d$ determined for membrane A reflects the errors inherent in the evaluation of these two parameters from data for the observed sieving coefficient obtained in the stirred apparatus. Our results could not confirm the existence of a concentration dependence for either S_∞ or $\epsilon\phi K_d$, although it should be noted that the protein concentration at the membrane surface (C_w) is actually a complex function not only of C_b but also of the filtrate flux and mass transfer coefficient. The variability in the values for S_∞ (0.021 to 0.12) and $\epsilon\phi K_d$ (3.9×10^{-3} to 7.0×10^{-3}) for the different 100-K membranes is similar to that reported previously for protein uptake and hydraulic permeability (Robertson and Zydney, 1990a) and for hindered diffusion (Robertson and Zydney, 1990b). Note that the somewhat larger values of S_∞ and $\epsilon\phi K_d$ obtained with membrane C are consistent with the somewhat larger permeability (L_p) of this membrane.

Experimental data for the observed and actual sieving coefficients for an OMEGA 50-K membrane (obtained at 600 rpm and 25 g/L) and an OMEGA 300-K membrane (obtained at 1,300 rpm and 25 g/L) are shown in Figures 2 and 3. Again there was no evidence of any membrane fouling during these experiments. The observed sieving coefficients for both membranes display the characteristic minimum arising from the competing effects of concentration polarization and the flux dependence of the actual sieving coefficient. The actual sieving coefficients decay monotonically to their asymptotic values of $S_\infty = 0.001$ for the 50-K membrane and $S_\infty = 0.48$ for the 300-K membrane. The solid curves are model calculations, with the best fit values of the parameters (S_∞ and $\epsilon\phi K_d$) determined as before and shown in Table 3. The agreement between model and data is excellent for both membranes, again indicating that the transport behavior is well described by Eqs. 3 and 16.

The best fit values, standard deviations, and correlation

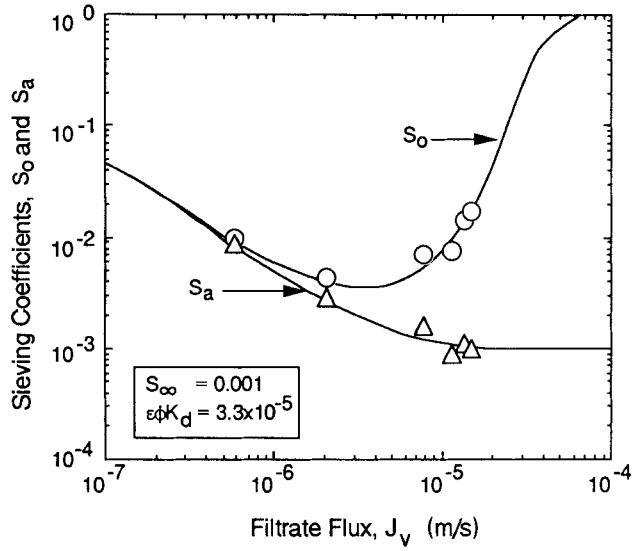

Figure 2. Observed and actual sieving coefficients for a 50-K membrane.

Solid curves represent model fit with parameters shown. $C_b = 25$ g/L and $k = 5.2 \times 10^{-6}$ m/s.

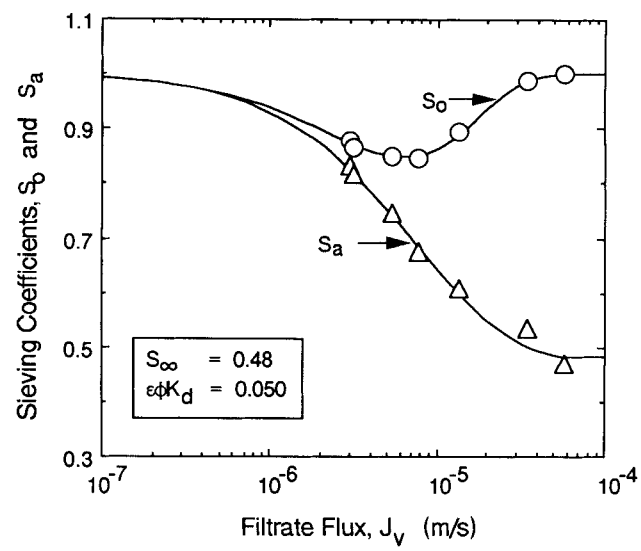

Figure 3. Observed and actual sieving coefficients for a 300-K membrane.

Solid curves represent model fit with parameters shown. $C_b = 25$ g/L and $k = 8.0 \times 10^{-6}$ m/s.

coefficients for S_∞ and $\epsilon\phi K_d$ for the different molecular weight cutoff membranes are summarized in Table 3 along with the measured values of the hydraulic permeability (L_p). The standard deviations were determined from the fit to the S_o data for a single membrane; the variability between membranes was substantially larger as shown in Table 2. The standard deviations for all the parameters were quite small, and the mean square deviations were all less than 15%. The high correlation coefficients between S_∞ and $\epsilon\phi K_d$ for the 300-K and 1-M membranes reflects the difficulty in fitting both of these parameters independently when the S_o data are all relatively close to unity. Both S_∞ and $\epsilon\phi K_d$ increase with increasing membrane molecular weight cutoff, with $\epsilon\phi K_d$ having a much greater dependence than S_∞.

Also shown in Table 3 are results obtained with two 0.01-μm track-etched polycarbonate membranes, one used at a bulk protein concentration of 25 g/L (membrane *A*) and one at 5 g/L (membrane *B*). Values for $\epsilon\phi K_d$ could not be determined for these membranes because of the difficulty in obtaining data in the flux-dependent regime for S_a due to the large value of δ_m (6 μm) and the very small porosity ($\epsilon < 0.01$). In addition, the membrane permeability decayed significantly over the course of these experiments, similar to the fouling behavior reported previously by Mitchell and Deen (1986) for small-pore track-etched membranes. The slightly larger value of S_∞ for membrane *B* may reflect a slightly larger pore size for this membrane, which would be consistent with the larger value of the permeability. The asymptotic sieving coefficients for the 0.01-μm polycarbonate membranes were slightly smaller than those obtained with the 300-K polyethersulfone membrane. These effects are discussed in more detail in the following section.

Comparison with hydrodynamic theory

To compare our experimental data for the hindered diffusion coefficient (ϕK_d) with hydrodynamic predictions, it is first necessary to evaluate the porosity of the membrane skin. The skin porosity for the native polyethersulfone membranes (ϵ_o) is 0.8 as provided by the manufacturer. The porosity after protein adsorption was evaluated from experimental data for protein uptake by the polyethersulfone membranes (Robertson and Zydney, 1990a) as:

$$\epsilon = \epsilon_o - \frac{m}{\rho_p A \delta_m} \tag{19}$$

where m is the mass of protein adsorbed in the skin layer of

Table 3. Transport Parameters for Different Molecular Weight Cutoff Polyethersulfone and Track-Etched Polycarbonate Membranes

Membrane	L_p ($m \times 10^{12}$)	S_∞	$\epsilon\phi K_d$ ($\times 10^2$)	Correlation Coefficient	Mean Deviation (*E*)
50-K	0.93	0.001 ± 0.0001	0.0033 ± 0.0005	0.42	0.15
100-K	2.0	0.037 ± 0.004	0.40 ± 0.02	0.67	0.08
300-K	4.1	0.48 ± 0.05	5.0 ± 0.7	0.98	0.01
1-M	5.9	0.58 ± 0.10	5.1 ± 1.8	0.96	0.03
0.01-μm (A)	0.03	0.28 ± 0.01	—	—	0.03
0.01-μm (B)	0.04	0.37 ± 0.02	—	—	0.07

Table 4. Porosity (ϵ), Specific Surface Area (s), and Equivalent Size Ratio (λ') for the Polyethersulfone Membranes

Membrane	ϵ	s (Å)	λ'
50-K	0.77 ± 0.05	11 ± 0.4	0.83 ± 0.01
100-K	0.51 ± 0.06	20 ± 1.2	0.64 ± 0.02
300-K	0.25 ± 0.10	41 ± 8.1	0.39 ± 0.06
1 M	0.50 ± 0.16	34 ± 5.5	0.44 ± 0.05

the membrane, ρ_p is the density of BSA (1.34×10^3 kg/m^3), and A is the membrane cross-sectional area. The mass of adsorbed protein in the skin was evaluated from data for the total protein uptake by subtracting off the contributions of the membrane substructure and matrix as described elsewhere (Robertson and Zydney, 1990a). The calculated values of the skin porosity for the different polyethersulfone membranes are shown in the second column of Table 4. Differences in porosity for the different molecular weight cutoff membranes reflect the differences in pore accessibility and pore surface area as discussed by Robertson and Zydney (1990a,b).

The best fit values for the hindered diffusion coefficient (ϕK_d), evaluated from the $\epsilon\phi K_d$ values in Tables 2 and 3 with the porosity given in Table 4, are plotted in Figure 4 as a function of S_∞ for the different polyethersulfone membranes. The error bars represent the standard deviations in the parameters as given in Table 3. No error bars are shown for the 50-K and 100-K membranes since they were quite small and lie within the range covered by the symbols. According to hydrodynamic theory, the hindered diffusion coefficient (ϕK_d) and the asymptotic sieving coefficient (S_∞) are unique functions of λ, with the specific functionality determined by the detailed pore geometry and the magnitude of any long-range interactions. The solid lines in Figure 4 are the predicted dependence of ϕK_d on S_∞ for spherical solutes in cylindrical (Eqs. 7 to 10) and slit-shaped (Eqs. 11 to 13) pores, in both cases neglecting

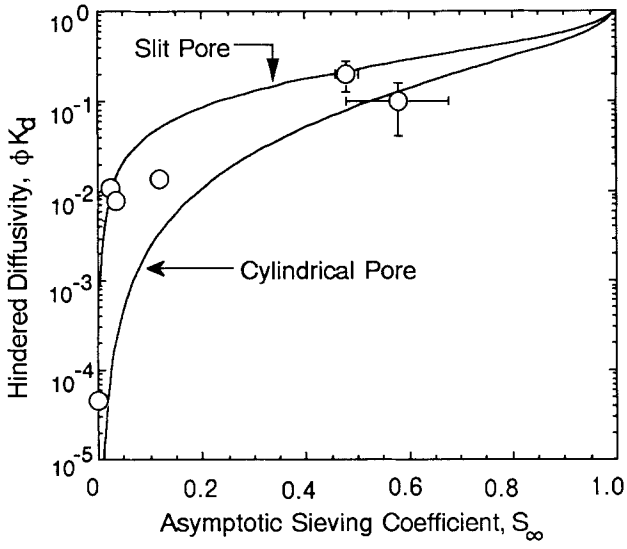

Figure 4. Best fit values for the hindered diffusivity as a function of the asymptotic sieving coefficient.

Solid curves are for spherical solutes in cylindrical (Eqs. 7 to 10) and slit-shaped (Eqs. 11 to 13) pores.

electrostatic interactions. The data are bounded by the two curves, indicating that available hydrodynamic models for hindered transport through idealized pores are able to provide important insights into the transport of globular proteins like BSA through the highly irregular pores characteristic of asymmetric ultrafiltration membranes.

Since no data were available for the detailed pore morphology and pore size distribution in the OMEGA membranes, it was not possible to rigorously compare our results with *a priori* predictions for S_∞ and ϕK_d. The situation is complicated further by the lack of any rigorous model for sieving or hindered diffusion for nonspherical solutes in even the simplest pore geometries. We thus chose to compare our experimental results with predictions of hydrodynamic theory using a semi-quantitative analysis developed by Robertson and Zydney (1990b). The partition coefficients for BSA in the different molecular weight cutoff membranes were evaluated using the model developed by Giddings et al. (1968) for partitioning of rigid solutes in a porous network formed by random intersecting parallel planes (Eq. 15). This model accounts for the presence of a pore size distribution in the membrane through the evaluation of ϕ, and it accounts for the ellipsoidal shape of BSA through the evaluation of the mean projected solute radius:

$$\frac{R^*}{b} = \frac{1}{4} + \frac{1}{4\alpha(\alpha^2-1)^{1/2}} \ln[\alpha + (\alpha^2-1)^{1/2}] \tag{20}$$

where b is the major axis and α the aspect ratio. For BSA, $b = 139$ Å and $\alpha = 3.56$ (Cooney, 1976) giving a mean projected solute radius of 40.3 Å. The specific pore surface area (s) was evaluated from the permeability of the membrane skin (L_p) using the Kozeny-Carman equation:

$$L_p = \frac{\epsilon s^2}{k_1 \delta_m} \tag{21}$$

where the Kozeny constant (k_1) is typically about 5 for a random porous media (Macdonald et al., 1979) and $k_1 = 2$ for a system with true cylindrical pores. All calculations reported in this manuscript employed $k_1 = 2$. The hydraulic permeability of the skin was evaluated from data for the overall permeability by subtracting off the contributions from the substructure and matrix as described by Robertson and Zydney (1990a).

The equilibrium partition coefficients for the different molecular weight cutoff membranes were evaluated directly from Eq. 15 using the results for the specific surface area of the pore. The size ratio for an equivalent spherical solute in a cylindrical pore (λ') was then evaluated from the partition coefficient using Eq. 9:

$$\lambda' = 1 - \sqrt{\phi} \tag{22}$$

with the results summarized in the last column of Table 4. [Note that Robertson and Zydney (1990b) evaluated R^* as the mean projected solute diameter instead of the radius, but then used this value in Eq. 15 as if it were the radius; this resulted in a factor of two error in their values for λ^* and a corresponding error in both ϕ and λ'.]

The experimental data for S_∞ and ϕK_d are plotted in Figure

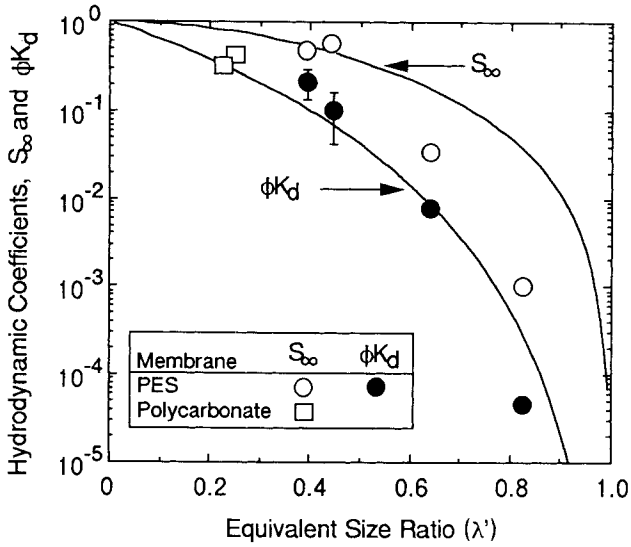

Figure 5. Comparison of experimental results for hindered diffusion (ϕK_d) and sieving (S_∞) with hydrodynamic predictions (Eqs. 7 to 10).

5 as a function of the equivalent size ratio λ'. The solid lines represent the theoretical predictions evaluated from the hydrodynamic analysis of Bungay and Brenner (1973) for spherical solutes in cylindrical pores, with λ replaced by the equivalent size ratio λ' in Eqs. 7 to 10. The data for the hindered diffusion coefficient are in relatively good agreement with the theory, with the values for the large-pore membranes slightly above the theoretical curve while that for the 50-K membrane is slightly below the theory. Very similar results would be obtained using the Stokes-Einstein radius for BSA (36 Å), since it is only slightly smaller than the mean projected solute radius ($R^* = 40.3$ Å) used in our analysis.

The S_∞ values for the 300-K and 1-M membranes are also in relatively good agreement with the model, but the sieving results for the 50-K and 100-K membranes fall well below the predicted curve. Note that if a larger value of the Kozeny constant were employed in the calculations, the data for both S_∞ and ϕK_d would be shifted to smaller λ', increasing the discrepancy between the theory and data for the 50-K and 100-K membranes. The unexpectedly small values of S_∞ for the 50-K and 100-K membranes may be due to the presence of a substantial number of very small pores which are inaccessible to protein but still permit significant solvent flow. This "excess" solvent flow would reduce the apparent value of the asymptotic sieving coefficient while leaving the hindered diffusion coefficient in the "open" pores largely unaffected. Note that this effect may be influenced significantly by BSA adsorption in these small molecular weight cutoff membranes, which would tend to "block" a significant number of pores to subsequent protein transport but still leave them accessible to solvent flow, a phenomenon suggested by Robertson and Zydney (1990b) in their analysis of hindered protein diffusion.

Also shown in Figure 5 are the S_∞ values for the 0.01-μm polycarbonate membranes. The effective pore radii for these membranes were calculated directly from the membrane permeability in Table 3 assuming Poiseuille flow using the pore density provided by the manufacturer (6×10^{12} pores/m^2). This gave a pore radius of about 0.015 μm, substantially larger than

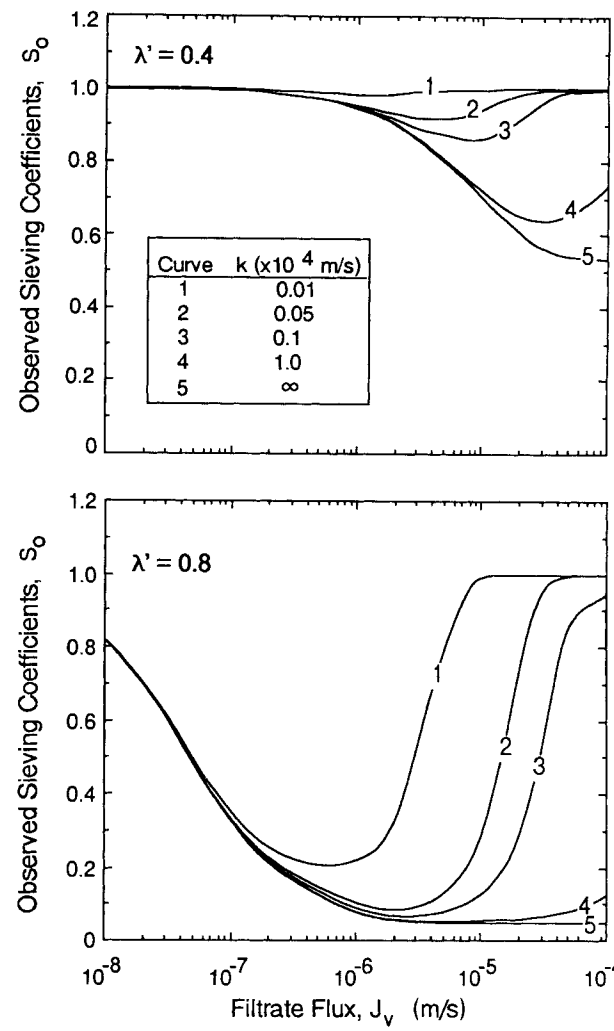

Figure 6. Model predictions for observed sieving coefficient vs. filtrate flux for several mass transfer coefficients for $\lambda' = 0.4$ (top panel) and $\lambda' = 0.8$ (bottom panel).

the nominal pore radius given by the manufacturer, but similar to the pore radii evaluated by Mitchell and Deen (1986) for Nuclepore track-etched polycarbonate membranes. The equivalent size ratio was then evaluated as the ratio of the mean projected solute radius (R^*) to the cylindrical pore radius (R_p). The best fit values for S_∞ were below the hydrodynamic predictions, similar to the behavior reported by Mitchell and Deen (1986) for BSA sieving through track-etched membranes. The reason for this discrepancy is unclear, but it may be due to electrostatic interactions between the adsorbed BSA and the BSA in solution as suggested by Mitchell and Deen (1986).

Implications for protein separations

The dependence of the actual and observed sieving coefficients on filtrate flux can have important implications in the design and analysis of clinical and/or industrial membrane devices. A detailed investigation of device design is beyond the scope of this study, but some of the more significant phenomena are illustrated in Figure 6. The solid lines represent the model predictions for the observed sieving coefficient at several

values of the mass transfer coefficient for $\lambda' = 0.4$ (upper panel) and $\lambda' = 0.8$ (lower panel). The model predictions for $k \to \infty$ are equivalent to the actual sieving coefficient since there are no bulk mass transfer limitations in this limit. The parameters S_∞ and ϕK_d were evaluated using Eqs. 7 to 10, giving $S_\infty = 0.53$ and $\phi K_d = 0.1$ for $\lambda' = 0.4$, and $S_\infty = 0.05$ and $\phi K_d = 5 \times 10^{-4}$ for $\lambda' = 0.8$. The skin porosity and thickness were assumed to be $\epsilon = 0.6$ and $\delta_m = 0.5$ μm, both characteristic of the asymmetric membranes examined in this study.

The observed sieving coefficients for both λ' display the characteristic minimum arising from the competing effects of a flux-dependent actual membrane sieving coefficient and bulk concentration polarization. Increasing the bulk mass transfer coefficient causes the minimum to shift to a higher flux, with the value of S_o at this point decreasing and eventually approaching S_∞ as $k \to \infty$. Increasing λ' causes the minimum in S_o to shift to a lower flux due to the increase in the ratio of $S_\infty/\phi K_d$ with increasing λ'. For these conditions, the minimum in the observed sieving coefficient is essentially equal to S_∞ above $k = 5 \times 10^{-5}$ m/s at $\lambda' = 0.8$, but a mass transfer coefficient well above 10^{-4} m/s is required for S_o to equal S_∞ for $\lambda' = 0.4$.

The flux at which the minimum in S_o occurs can be evaluated analytically by expressing S_o in terms of S_∞ and $\epsilon\phi K_d$ using Eqs. 16 and 3 and then setting the derivative of this expression with respect to J_v equal to zero yielding:

$$J_v = \frac{k}{Pe^*} \ln(1 + Pe^*) \tag{23}$$

where Pe^* is the membrane Peclet number based on the bulk mass transfer coefficient:

$$Pe^* = \left(\frac{S_\infty}{\epsilon\phi K_d}\right)\left(\frac{k\delta_m}{D_\infty}\right) \tag{24}$$

For small values of Pe^*, Eq. 23 reduces to $J_v = k$, independent of the membrane properties, while at large Pe^* the minimum occurs at $J_v < k$.

The value of the actual sieving coefficient at the minimum in S_o can be calculated directly from Eq. 3 with the flux given by Eq. 23 as:

$$S_a = \frac{S_\infty(1 + Pe^*)}{S_\infty + Pe^*} \tag{25}$$

Thus, even at the minimum in S_o, the actual sieving coefficient is equal to S_∞ only if $Pe^* \gg 1$. This condition is relatively easy to satisfy with most track-etched membranes since ϵ is very small (< 0.01) and δ_m is on the order of 10 μm. The situation is very different for the asymmetric membranes (Figure 6) due to the large porosity and the very small skin thickness ($\delta_m \approx 0.5$ μm). For $\lambda' = 0.4$, the mass transfer coefficient would have to be greater than 10^{-4} m/s, a condition that could not be obtained in our stirred cell due to the inherent limitations on the stirring speed. This constraint on Pe^* is also difficult to satisfy in cross-flow membrane devices, with $k > 10^{-4}$ m/s corresponding to a wall shear rate greater than 10^6 s^{-1} as given by the Leveque solution for the mass transfer coefficient for a device 0.1 m long. Thus, considerable care must be taken in interpreting published results for the sieving coefficients of asymmetric ultrafiltration membranes, many of which may be far above S_∞ due to the effects of solute diffusion and bulk mass transport. The diffusional contribution to the flux is much less significant for very small pore membranes, as seen in the lower panel of Figure 6, since the ratio of $S_\infty/\phi K_d$ increases significantly at large λ' (becoming infinitely large in the limit of $\lambda' = 1$).

The flux dependence of the actual sieving coefficient can have important implications in the development of membrane devices for the fractionation of multicomponent protein solutions. Increasing solute size, that is, increasing λ', causes a reduction in S_∞, but it increases the value of $S_\infty/\phi K_d$ due to the more rapid decrease in ϕK_d with increasing λ'. This increase in $S_\infty/\phi K_d$ causes the actual sieving coefficient to decay toward its asymptotic value at a lower filtrate flux. This leads to a maximum in the intrinsic membrane selectivity, defined as the ratio of S_a for the two solutes, at a flux where the actual sieving coefficient of the larger solute is close to S_∞ while that for the smaller solute is still close to one due to the large diffusional contribution for the smaller protein. To accurately model this type of protein separation one would also need to account for the variation in D_∞, and in turn the mass transfer coefficient, with solute size, but these effects are actually much smaller than those associated with the differences in λ' (shown in Figure 6) due to the strong dependence of the hindered transport parameters (S_∞ and $\epsilon\phi K_d$) on solute size. The flux dependence of the actual sieving coefficient thus causes the ratio of S_a at $\lambda' = 0.4$ to S_a at $\lambda' = 0.8$ to go through a maximum of about 17 at $J_v = 3.3 \times 10^{-6}$ m/s before decaying to an asymptotic value of about 11 at very high flux. This phenomenon has not been generally appreciated in previous studies of selective filtration, although it can potentially lead to substantial improvements in the intrinsic selectivity of membrane fractionation devices.

Discussion

The experimental data obtained in this study provide the most complete results currently available for combined convective and diffusive transport of a globular protein like BSA through asymmetric ultrafiltration membranes. The data clearly indicate that the flux dependence of the actual membrane sieving coefficient is well described by Eq. 3, with the asymptotic value of the sieving coefficient not obtained until very high fluxes, often well above those encountered in typical industrial or clinical applications. This suggests that much of the data previously reported for the sieving coefficient of asymmetric ultrafiltration membranes may be substantially larger than S_∞, and in some instances it may be impossible to measure S_∞ directly due to the combined effects of a flux-dependent actual sieving coefficient and bulk concentration polarization. The flux dependence of the actual sieving coefficient can also be important in determining the intrinsic selectivity of membrane devices for protein fractionation, although this phenomenon has not been exploited in most previous studies of selective filtration.

The calculated values for S_∞ and ϕK_d for these asymmetric polyethersulfone membranes were also shown to be in relatively good agreement with predictions of available hydrodynamic models for spherical solutes in cylindrical pores with the equiv-

alent solute to pore size ratio evaluated using the partitioning model developed by Giddings et al. (1968). This model explicitly takes into account the ellipsoidal shape of BSA through the evaluation of the mean projected solute radius R^*, as well as the presence of a pore size distribution within the membrane through the evaluation of ϕ and in turn λ'. In addition, the model directly accounts for the effect of protein adsorption by evaluating the pore volume to surface area ratio from data for the hydraulic permeability of the membrane skin after equilibrium protein adsorption. This good agreement demonstrates that available hydrodynamic models can provide important insights into protein transport through the highly constricted pores in asymmetric ultrafiltration membranes and can even provide good *a priori* predictions of the hindrance factors for convective and diffusive transport simply from experimental measurements of the membrane hydraulic permeability.

Limbach and Wei (1990) have recently obtained data for the hindered diffusion of small ellipsoidal solutes through granular catalyst particles which were also in good agreement with hydrodynamic models for spherical solutes in cylindrical pores. Limbach and Wei (1990) evaluated the effective solute size for partitioning as the mean projected solute radius, while that for the hindrance factor (K_d) was taken as the hydrodynamic radius. Note that for BSA, the mean projected solute radius and the hydrodynamic radius differ by less than 10%. Limbach and Wei (1990) evaluated the effective pore size from the ratio of the pore volume to surface area as in our analysis. The partition coefficient and hindrance factor were then evaluated using available hydrodynamic models for spherical solutes in cylindrical pores. For partitioning, this corresponds to using λ^* instead of λ in Eq. 9. For small values of λ^*, Limbach and Wei's approach is essentially equivalent to our analysis, since the first two terms in the Taylor series expansions for Eqs. 9 and 15 are identical. For large values of λ^*, the two analyses predict substantially different behavior; the partition coefficient evaluated by Limbach and Wei (1990) becomes zero in the limit $\lambda^* = 1$, while our analysis gives $\phi = 0.135$ under these conditions with $\phi \to 0$ only as $\lambda^* \to \infty$. This sharp discrepancy arises from our use of the partitioning model developed by Giddings et al. (1968), which explicitly accounts for the presence of a broad pore size distribution with the largest pores permitting transport of even relatively large solutes. Limbach and Wei's (1990) experimental data were limited to $\lambda^* < 0.25$ (with a single data point at $\lambda^* = 0.44$); however, our experimental data for BSA transport in the OMEGA 50-k and 100-k membranes corresponded to $\lambda^* = 1.78$ and 1.02, respectively, and under these conditions Limbach and Wei's approach would predict that both S_∞ and ϕK_d are zero.

The good agreement between our experimental data for BSA transport and available hydrodynamic models is in sharp contrast to the results obtained by Nakao and Kimura (1981) and Tsapuik et al. (1990) for the transport of small solutes and flexible polymers through ultrafiltration membranes. Both Nakao and Kimura (1981) and Tsapuik et al. (1990) reported a variation in the apparent membrane thickness with solute size, which they attributed to the extensive pore connectivity in the asymmetric membranes. Our results provide no evidence for such an effect.

Our results for BSA transport through the OMEGA 50-k membrane are in good agreement with BSA sieving results obtained previously by Robertson and Zydney (1988) using an unstirred batch filtration device. Robertson and Zydney (1988) found that the flux dependence of the actual sieving coefficient, evaluated by comparison of the filtrate concentration data with an integral solution to the unsteady diffusion equation in the unstirred device, was in good agreement with Eq. 3 with $S_\infty = 0.010 \pm 0.001$ and $\epsilon\phi K_d = 4.4 \pm 0.3 \times 10^{-5}$. This value for $\epsilon\phi K_d$ is in good agreement with that obtained in this study (3.3×10^{-5}), but the value for S_∞ is somewhat larger than that shown in Table 3 although it is still within the range of variability expected for the very small-pore 50-K membrane. Robertson and Zydney could not evaluate both S_∞ and $\epsilon\phi K_d$ for the larger-pore membranes in the unstirred device due to the very high degree of concentration polarization, but experimental data for the 100-K membrane gave $S_\infty \approx 0.03$ (Robertson, 1989), in excellent agreement with the results reported in this study. In contrast, S_∞ for the 1-M membrane was about 0.04, substantially smaller than the value shown in Table 3. This discrepancy was probably due to protein deposition on the membrane surface in the unstirred filtration experiments, which employed unfiltered BSA solutions instead of the filtered protein solutions used in the current investigation.

Experimental data for the hindered diffusion coefficient for BSA through the OMEGA membranes were obtained by Robertson and Zydney (1990b) using a well stirred diffusion cell, with the overall resistance to diffusion through the skin + substructure + matrix evaluated from the flux of radiolabeled BSA across the membrane as a function of time. The diffusional resistance provided by the membrane skin, equal to the ratio of the membrane thickness to the effective diffusivity, was then evaluated by subtracting off the contributions of the matrix, determined from independent measurements using isolated matrices, and the substructure, with the latter value estimated from the results obtained with the matrix. The hindered diffusion coefficient in the skin was then calculated from the skin resistance using the skin porosity and thickness as done in the current study. Results for the 50-K membrane gave $\phi K_d = 1.3 \pm 0.7 \times 10^{-5}$ (Robertson and Zydney, 1990b), which is only slightly smaller than the value obtained in this study. In contrast, their results for the OMEGA 100-K membrane ($\phi K_d = 2.5 \pm 1.9 \times 10^{-5}$) were two orders of magnitude smaller than that obtained in this study, while their results for the OMEGA 300-K and 1-M membranes ($\phi K_d = 2.2 \pm 1.6 \times 10^{-5}$ and $\phi K_d = 5.5 \pm 1.5 \times 10^{-5}$, respectively) were almost three orders of magnitude smaller than those reported in Table 3.

The reasons for the large discrepancy in the hindered diffusion coefficients obtained from our sieving experiments and the diffusion experiments of Robertson and Zydney (1990b) are unclear, although there are several possible explanations. The data obtained in the diffusion experiments were evaluated from the overall diffusional resistance of the membrane, equal to the sum of the diffusional resistances provided by each region of the membrane. Thus, even though the effective diffusivities in the substructure and matrix are significantly greater than those in the skin (due to the much larger pore size), the diffusional resistance provided by these regions is still substantial since the substructure and matrix are both several orders of magnitude thicker than the skin (50 μm for the substructure and 230 μm for the matrix compared to 0.5 μm for the skin). Since the skin resistance was evaluated by sub-

tracting off the contributions of the matrix and substructure, relatively small errors in the evaluation of these resistances (for example, a factor of 2 or 3) could have caused very large deviations in the hindered diffusion coefficient in the skin (as much as 2 to 3 orders of magnitude). This is in sharp contrast to the analysis of our sieving data, in which the results are very heavily weighted by the properties of the upper skin layer. For example, for a simple two-layer model of the membrane (skin + support), the actual sieving coefficient is given as (Jagur-Grodzinsky and Kedem, 1966):

$$S_a = \frac{S_{\infty 1}\exp(Pe_{m1})S_{\infty 2}\exp(Pe_{m2})}{S_{\infty 2}\exp(Pe_{m2})[\exp(Pe_{m1})-1]+S_{\infty 1}[\exp(Pe_{m2})-1+S_{\infty 2}]} \tag{26}$$

where $S_{\infty 1}$ and $S_{\infty 2}$ and Pe_{m1} and Pe_{m2} are the asymptotic sieving coefficients and membrane Peclet numbers for the upper (skin) and lower (support) layers of the membrane, respectively. When $S_{\infty 2}$ is close to one, as would be expected for the highly porous support structure, Eq. 26 reduces to Eq. 3 irrespective of the thickness of the lower layer, with the sieving properties of the composite membrane (both S_∞ and ϕK_d) determined entirely by the properties of the upper layer.

This difference in the "weighting" of the upper and lower regions of the membrane implies that any axial variation in pore size within the membrane skin will manifest itself differently in the sieving and diffusion experiments, with the properties of the uppermost region of the skin being more heavily weighted in the sieving experiments than in the diffusion experiments. In addition, the presence of a radial pore size distribution (on the membrane surface) will have different affects on the sieving and diffusion experiments, since the sieving results are weighted by the fluid flow rate through each pore (proportional to R_p^4) while the diffusion results are weighted only by the pore area (proportional to R_p^2). Thus, the discrepancy in the values of $\epsilon\phi K_d$ determined from the diffusion and sieving experiments could be due, at least in part, to the presence of a broad pore size distribution, either axially or radially, in the skin of the asymmetric polyethersulfone membranes.

Acknowledgment

This work was supported in part by Grant CTS-8812943 from the National Science Foundation and by Grant RO1 HL39455-02 from the Public Health Service. The authors would also like to acknowledge Filtron Corporation for their donation of the OMEGA membranes and Suzanne Wanalista for her assistance with the sieving experiments.

Notation

A = membrane cross-sectional area
A_2, A_3 = expansion coefficients for evaluation of protein osmotic pressure
a_n, b_n = expansion coefficients in hydrodynamic model (values in Table 1)
b = major axis of ellipsoid
C_b = bulk protein concentration
C_f = filtrate concentration
C_s = radially averaged solute concentration in pore
C_w = wall concentration
D_{eff} = effective pore diffusivity ($\phi K_d D_\infty$)
D_∞ = free solution diffusion coefficient
E = mean square deviation
h = slit half width
J_v = superficial velocity
k = bulk mass transfer coefficient
k_1 = Kozeny constant
K_c = hindrance factor for convection
K_d = hindrance factor for diffusion
K_s, K_t = hydrodynamic functions in Bungay and Brenner's analysis
L_p = membrane hydraulic permeability
m = mass of adsorbed protein
M_p = protein molecular weight
N = number of data points
N_s = solute flux across membrane
Pe^* = membrane Peclet number based on bulk mass transfer coefficient
Pe_m = membrane Peclet number
r = radius of stirred cell
R = actual membrane rejection coefficient ($1 - S_a$)
R^* = mean projected solute radius
Re = Reynolds number ($\omega r^2/\nu$)
R_p = pore radius
R_s = solute radius
s = ratio of pore volume to pore surface area
S_a = actual sieving coefficient (C_f/C_w)
Sc = Schmidt number (ν/D_∞)
S_o = observed sieving coefficient (C_f/C_b)
S_p = pore surface area
S_∞ = high flux asymptotic sieving coefficient
T = absolute temperature
V = solution velocity in pore
V_p = pore volume
z = axial position in pore

Greek letters

α = aspect ratio of ellipsoid
δ_m = membrane thickness
ΔP = pressure drop across membrane
ϵ = membrane porosity after adsorption
ϵ_o = porosity of clean membrane
ϕ = partition coefficient
λ = ratio of solute radius to pore radius (R_s/R_p) or slit half-width (R_s/h)
λ' = equivalent size ratio
λ^* = effective size ratio ($R^*/2s$)
Π = protein osmotic pressure
ρ_p = protein density
σ_o = osmotic reflection coefficient
ν = kinematic viscosity
Ψ = coefficient in mass transfer correlation
ω = stirrer speed

Literature Cited

Adamski, R. P., and J. L. Anderson, "Solute Concentration Effects on Osmotic Reflection Coefficient," *Biophys. J.*, **44**, 7 (1983).

Anderson, J. L., "Configurational Effect on the Reflection Coefficient for Rigid Solutes in Capillary Pores," *J. Theor. Biol.*, **90**, 405 (1981).

Anderson, J. L., and J. A. Quinn, "Restricted Transport in Small Pores: a Model for Steric Exclusion and Hindered Particle Motion," *Biophys. J.*, **14**, 130 (1974).

Baltus, R. E., and J. L. Anderson, "Hindered Diffusion of Asphaltenes through Microporous Membranes," *Chem. Eng. Sci.*, **38**, 1959 (1983).

Beck, E. E., and J. S. Schultz, "Hindrance of Solute Diffusion within Membranes as Measured with Microporous Membranes of Known Pore Geometry," *Biochim. Biophys. Acta*, **225**, 273 (1972).

Blatt, W. F., A. Dravid, A. S. Michaels, and L. Nelson, "Solute Polarization and Cake Formation in Membrane Ultrafiltration: Causes, Consequences, and Control Techniques," *Membrane Science and Technology*, J. E. Flinn, ed., Plenum Press, New York (1970).

Bohrer, M. P., G. D. Patterson, and P. J. Carroll, "Hindered Diffusion of Dextran and Ficoll in Microporous Membranes," *Macromol.*, **17**, 1170 (1984).

Brenner, H., and L. J. Gaydos, "The Constrained Brownian Movement of Spherical Particles in Cylindrical Pores of Comparable Radius," *J. Colloid Interf. Sci.*, **58**, 313 (1977).
Bungay, P. M., and H. Brenner, "The Motion of a Closely Fitting Sphere in a Fluid Filled Tube," *Int. J. Multiph. Flow*, **1**, 25 (1973).
Cooney, D. O., *Biomedical Engineering Principles: An Introduction to Fluid, Heat and Mass Transport Processes*, Marcel-Dekker, New York (1976).
Deen, W. M., "Hindered Transport of Large Molecules in Liquid-Filled Pores," *AIChE J.*, **33**, 1409 (1987).
Deen, W. M., M. P. Bohrer, and N. B. Epstein, "Effects of Molecular Size and Configuration on Diffusion in Microporous Membranes," *AIChE J.*, **27**, 952 (1981).
Giddings, J. C., E. Kucera, C. P. Russell, and M. N. Myers, "Statistical Theory for the Equilibrium Distribution of Rigid Molecules in Inert Porous Networks: Exclusion Chromatography," *J. Phys. Chem.*, **72**, 4397 (1968).
Happel, J., and H. Brenner, *Low Reynolds Number Hydrodynamics*, Nijhoff, The Hague (1983).
Jagur-Grodzinsky, J., and O. Kedem, "Transport Coefficients and Salt Rejection in Uncharged Hyperfiltration Membranes," *Desalination*, **1**, 327 (1966).
Kedem, O., and A. Katchalsky, "Thermodynamic Analysis of Permeability of Biological Membranes to Non-Electrolytes," *Biochim. Biophys. Acta*, **27**, 229 (1958).
Keller, K. H., E. R. Canales, and S. H. Yum, "Tracer and Mutual Diffusion Coefficients of Proteins," *J. Phys. Chem.*, **75**, 379 (1971).
Lane, J. A, *Chemical Engineers' Handbook*, 3rd ed., R. H. Perry, ed., McGraw-Hill, New York (1950).
Lightfoot, E. N., *Transport Phenomena in Living Systems*, Wiley, New York (1974).
Limbach, K. W., J. M. Nitsche, and J. Wei, "Partitioning of Nonspherical Molecules between Bulk Solution and Porous Solids," *AIChE J.*, **35**, 42 (1989).
Limbach, K. W., and J. Wei, "Restricted Diffusion through Granular Materials," *AIChE J.*, **36**, 242 (1990).
Long, T. D., D. L. Jacobs, and J. L. Anderson, "Configurational Effects on Membrane Rejection," *J. Memb. Sci.*, **9**, 13 (1981).
Macdonald, I. F., M. S. El-Sayes, K. Mow, and F. A. L. Dullien, "Flow Through Porous Media: The Ergun Equation Revisited," *Ind. Eng. Chem. Fundam.*, **18**, 199 (1979).
Malone, D. M., and J. L. Anderson, "Diffusional Boundary Layer Resistances for Membranes with Low Porosity," *AIChE J.*, **23**, 177 (1977).
Mavrovouniotis, G. M., and H. Brenner, "Hindered Sedimentation, Diffusion, and Dispersion Coefficients for Brownian Spheres in Circular Cylindrical Pores," *J. Colloid Interf. Sci.*, **124**, 169 (1988).
Mitchell, B. D., and W. M. Deen, "Effect of Concentration on the Rejection Coefficients of Rigid Macromolecules in Track-Etch Membranes," *J. Colloid Interf. Sci.*, **113**, 132 (1986).
Mitchell, B. D., and W. M. Deen, "Theoretical Effects of Macromolecule Concentration and Charge on the Rejection Coefficients of Rigid Macromolecules in Track-Etch Membranes," *J. Memb. Sci.*, **19**, 75 (1984).
Munch, W. D., L. P. Zestar, and J. L. Anderson, "Rejection of Polyelectrolytes from Microporous Membranes," *J. Memb. Sci.*, **5**, 77 (1979).
Nakao, S., and S. Kimura, "Analysis of Solutes Rejection in Ultrafiltration," *J. Chem. Eng. Japan*, **14**, 32 (1981).
Oda, T., and N. Inoue, "New Technology for Plasma Separation," *Plasmapheresis*, Y. Nose, P. S. Machelsky, and J. W. Smith, eds., ISAO Press, Cleveland (1983).
Opong, W. S., and A. L. Zydney, "Hydraulic Permeability of Deposited Protein Layers Formed during Ultrafiltration," *J. Colloid Interf. Sci.*, **142**, 41 (1991).
Renkin, E., "Filtration, Diffusion, and Molecular Sieving through Porous Cellulose Membranes," *J. Gen. Physiol.*, **38**, 225 (1954).
Robertson, B. C., "A Mass Transfer Analysis of Selective Protein Filtration with Applications to Plasma Exchange Therapy," PhD Thesis, Univ. of Delaware (1989).
Robertson, B. C., and A. L. Zydney, "Protein Adsorption in Asymmetric Ultrafiltration Membranes with Highly Constricted Pores," *J. Colloid Interf. Sci.*, **134**, 563 (1990a).
Robertson, B. C., and A. L. Zydney, "Hindered Protein Diffusion in Asymmetric Ultrafiltration Membranes with Highly Constricted Pores," *J. Memb. Sci.*, **29**, 287 (1990b).
Robertson, B. C., and A. L. Zydney, "Stefan-Maxwell Analysis of Protein Transport in Porous Membranes," *Sep. Sci. Technol.*, **23**, 1799 (1988).
Rodilosso, P. D., "Determination of Partition Coefficient of Macromolecules in Porous Media: Potential Flows of Mass and Charge about Solute Obstacles in Model Membranes," PhD Thesis, Univ. of Pennsylvania (1984).
Schultz, J. S., R. Valentine, and C. Y. Choi, "Reflection Coefficients of Homopore Membranes: The Effect of Molecular Size and Configuration," *J. Gen. Physiol.*, **73**, 49 (1979).
Sieberth, H. G., W. M. Glockner, and H. Kierdorf, "Cascade Filtration for Macromolecular Separation," *Plasma Separation and Plasma Fractionation*, M. J. Lysaght and H. J. Gurland, eds., Karger, Basel (1983).
Smith, K. A., C. K. Colton, E. W. Merrill, and L. B. Evans, "Convective Transport in a Batch Dialyzer: Determination of the True Membrane Permeability from a Single Measurement," *AIChE Symp. Ser.*, **64**, 45 (1968).
Smith, III, F. G., and W. M. Deen, "Electrostatic Effects on Partitioning of Spherical Colloids between Bulk Solution and Cylindrical Pores," *J. Colloid Interf. Sci.*, **91**, 571 (1983).
Spiegler, K. S., and O. Kedem, "Thermodynamics of Hyperfiltration (Reverse Osmosis): Criteria for Efficient Membranes," *Desalination*, **1**, 311 (1966).
Tsapuik, E. A., M. T. Bryk, V. M. Kochkodan, and E. E. Danilenko, "Separation of Aqueous Solutions of Nonionic Organic Solutes by Ultrafiltration," *J. Memb. Sci.*, **48**, 1 (1990).
Vilker, V. L., C. K. Colton, and K. A. Smith, "The Osmotic Pressure of Concentrated Protein Solutions: Effect of Concentration and pH in Saline Solutions of Bovine Serum Albumin," *J. Colloid Interf. Sci.*, **79**, 548 (1981).
Wong, J., and J. A. Quinn, "Hindered Diffusion of Macromolecules in Track-Etched Membranes," *Colloid Interface Science*, Vol. 5, M. Kerker, ed., Academic Press, New York (1976).
Zeman, L., and M. Wales, "Steric Rejection of Polymeric Solutes by Membranes with Uniform Pore Size Distribution," *Sep. Sci. Technol.*, **16**, 275 (1981).

Appendix

The mass transfer coefficients in the stirred cell were evaluated by comparison of model calculations and experimental data for the flux of BSA solutions through highly retentive OMEGA polyethersulfone membranes as a function of applied pressure (ΔP). The experiments employed prefiltered BSA solutions, with the membranes pre-adsorbed with BSA for 24 hours prior to use. The apparatus and procedures were identical to those described earlier. Results for the 30-k and 50-k membranes are shown in Figure A1. At low pressures, the flux increased linearly with increasing pressure, with only a weak dependence on bulk concentration and stirring speed. At higher pressures, the flux increased more slowly due to the increase in protein osmotic pressure associated with the increase in concentration polarization. The flux increased with increasing stirring speed due to the reduction in concentration polarization and decreased with increasing bulk protein concentration due to the increase in osmotic pressure difference across the membrane.

The calculated values of the filtrate flux were determined using the Kedem and Katchalsky (1958) analysis:

$$J_v = L_p(\Delta P - \sigma_o \Delta \Pi) \tag{A1}$$

where σ_o is the osmotic reflection coefficient of the membrane, and $\Delta\Pi$ is the osmotic pressure difference across the membrane,

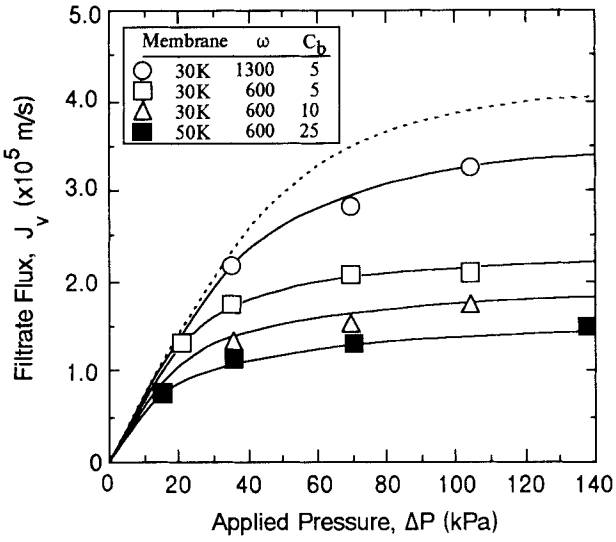

Figure A1. Comparison of experimental and calculated values of the filtrate flux for BSA filtration through highly retentive membranes.

Solid curves are model calculations using best fit values of the mass transfer coefficient as described in the text. Dashed curve is the model calculation at $\omega = 1{,}300$ rpm using the mass transfer coefficient given by the correlation developed by Smith et al. (1968) with $\Psi = 0.277$.

which was evaluated from the protein concentrations (C_w and C_f) using the correlation developed by Vilker et al. (1981):

$$\Pi = \frac{RT}{M_p}\left(C + A_2C^2 + A_3C^3\right) \tag{A2}$$

where $A_2 = 9.22 \times 10^{-3}$ L/g and $A_3 = 3.01 \times 10^{-5}$ (L/g)^2 at pH 7.4. The predicted values of J_v (and C_w) were evaluated by iterative solution of Eq. A1 and the stagnant film model:

$$J_v = k \ln\left(\frac{C_w - C_f}{C_b - C_f}\right) \tag{A3}$$

with the best fit values of the mass transfer coefficient determined by minimizing the sum of the squared residuals between experimental data and calculated values for the flux. Since the OMEGA 30-k membrane was fully retentive to BSA, $C_f = 0$ and $\sigma_o = 1$. Model calculations for the 50-k membrane used $\sigma_o = 0.99$ and the experimental values for the filtrate concentrations at each pressure; the best fit value for the mass transfer coefficient was unchanged using $0.95 < \sigma_o < 1.0$.

The solid curves in Figure A1 are the calculated flux using the best fit values of the mass transfer coefficients for each experimental run. The calculations are in very good agreement with the data at both stirring speeds and at all three bulk protein concentrations. The calculated values of the wall concentration in these experiments were all less than 400 g/L, which is below the solubility limit or gel concentration for BSA. In addition, saline flux measurements obtained after completion of the protein filtrations were essentially identical to those obtained prior to the experiments, indicating that protein deposition on the membrane surface was negligible. The dashed curve in Figure A1 is the calculated flux using the mass transfer coefficient given by the correlation developed by Smith et al. (1968) at $\omega = 1{,}300$ rpm ($k = 9.7 \times 10^{-6}$ m/s), which is about 20% higher than the best fit value at this stirring speed ($k = 8.0 \times 10^{-6}$ m/s). The calculated values for the filtrate flux using this mass transfer coefficient are uniformly higher than the experimental data, with the magnitude of this discrepancy being about 20% at the higher pressures. Similar behavior was observed at $\omega = 600$ rpm; the calculated curves using the mass transfer coefficient given by Smith et al. (1968) at this stirring speed were not shown for clarity.

The best fit values of the mass transfer coefficients at $\omega = 600$ rpm ranged from $5.0\text{–}5.4 \times 10^{-6}$ m/s, while that at $\omega = 1{,}300$ rpm was 8.0×10^{-6} m/s. These mass transfer coefficients are in excellent agreement with those calculated from Eq. 17 with $\Psi = 0.23$: $k = 5.2 \times 10^{-6}$ m/s at $\omega = 600$ rpm and $k = 8.0 \times 10^{-6}$ m/s at $\omega = 1{,}300$ rpm. This value of Ψ is about 17% less than the value ($\Psi = 0.277$) calculated using the correlations developed by Smith et al. (1968). These mass transfer coefficients are also consistent with the stirring speed dependence given by Eq. 17, although much more extensive data would be required to independently evaluate the *Re* exponent in this correlation. Equation 17, with $\Psi = 0.23$, was used to evaluate the mass transfer coefficients for our sieving experiments, all of which were performed at either $\omega = 600$ or 1,300 rpm.

Manuscript received Nov. 26, 1990, and revision received July 10, 1991.